magnetochemistry

MDPI

Article

Interface Effects on Magnetic Anisotropy and Domain Wall Depinning Fields in Pt/Co/AlO$_x$ Thin Films

Babu Ram Sankhi [1,*], Ujjal Lamichhane [1], Soumya Mandal [2], Ritesh Sachan [2], Emrah Turgut [1] and Derek Meyers [1]

[1] Department of Physics, Oklahoma State University, Stillwater, OK 74078-3072, USA
[2] Department of Mechanical and Aerospace Engineering, Oklahoma State University, Stillwater, OK 74078-3072, USA
* Correspondence: bsankhi@okstate.edu

Abstract: We report the dependence of the domain wall depinning field, domain wall velocity, including anisotropy direction, and magnetic properties on the oxidized aluminum thickness of perpendicularly magnetized asymmetric Pt/Co/AlO$_x$ trilayers. We also adopt the low-temperature magneto-transport measurement technique to investigate the amount of oxygen at the Co/AlO$_x$ interface of our magnetic thin films. At the lowest temperature of 25 K, it is found that the coercivity for the 5 nm aluminum thickness sample is very close to the average value and coercivity diminished above and below this critical aluminum thickness, hinting at a large variation in CoO$_x$ content at the interface. This tendency is also consistent with the modification of the depinning fields, coercive fields, and surface roughness measured at room temperature. Our results highlight an efficient way of controlling the depinning fields and other magnetic characteristics, which is important for stabilizing and driving magnetic spin textures and applicable to energy-efficient next-generation spintronics devices.

Keywords: interface; domain walls; perpendicular magnetic anisotropy; magneto-optical Kerr effect; depinning field; skyrmion

Citation: Sankhi, B.R.; Lamichhane, U.; Mandal, S.; Sachan, R.; Turgut, E.; Meyers, D. Interface Effects on Magnetic Anisotropy and Domain Wall Depinning Fields in Pt/Co/AlO$_x$ Thin Films. *Magnetochemistry* **2022**, *8*, 154. https://doi.org/10.3390/magnetochemistry8110154

Academic Editor: José Vergara

Received: 21 October 2022
Accepted: 10 November 2022
Published: 12 November 2022

1. Introduction

Perpendicularly magnetized magnetic ultrathin films with capabilities for data storage in memory and other recording media have been extensively studied for many years [1–3]. In earlier works, it has been established that perpendicular magnetic recording systems have a much higher storage capacity and better thermal stability compared to systems based on conventional longitudinal recording technology [1,4]. Hence, perpendicular magnetic anisotropic (PMA) films are widely applicable for next-generation low power, nonvolatile magnetic racetrack, and shift memories [5–7].

In such memory devices, magnetic spin textures, such as chiral domain walls (DW) and skyrmions, are the key ingredients, and their dynamics are crucial in storing the information in the form of bits. Study and manipulation of the depinning field that assists in moving such spin textures have received great attention. In the DW-based racetrack memories, the defects in the ultrathin films hinder their mobility, and the depinning field surpasses the DW energy consumption that provides the motion. Previously, it was assumed that the skyrmion-based memory system is likely less affected by the pinning centers because of the skyrmion's unique topological properties. However, the experimental results in ultrathin films performed by Yu et al. have shown the prominent effect of pinning centers even on the skyrmion motion as its size is much larger than the average distance between the neighboring pinning centers [6,8], further emphasizing the importance of the depinning field on magnetic memory applications.

In magnetic thin film structures, the interfaces are critical for various magnetic parameters and interactions, including PMA [9,10], the Dzyaloshinskii–Moriya interaction (DMI) [11,12], saturation magnetizations [13], and exchange bias and coercivity fields [14–16]. In the past few years, the dependence of annealing temperature and oxidation time on magnetic anisotropy in Pt/Co/AlO_x trilayers was experimentally observed [17,18]. Similarly, the comprehensive studies of current and field-induced DW dynamics [19–21], PMA, magneto-optical Kerr-effect, and DMI [11,22–24], due to the transformation of the Co/AlO_x interface, have been performed on Pt/Co/AlO_x material stacks. Recently, profound studies of electric field modulated DMI and spin-orbit torque (SOT) were done on the Pt/Co/AlO_x thin films, strengthening the importance of the ferromagnet (FM)/metal oxide (MO_x) boundary in low-power electronics [25,26]. However, the impact of the AlO_x layer on the magnetic properties along with the DW dynamics and depinning fields is still not known. Known properties of the Co/AlO_x interface have already been utilized for the construction of energy-efficient spin-based memory and logic devices [27–29], pointing to the importance of understanding the influence of the AlO_x layer on the magnetic properties.

In this paper, we present a novel method to optimize the DW depinning fields, velocity, and other magnetic properties by controlling the aluminum oxide thickness in Pt/Co/AlO_x trilayers. Additionally, the coercivities of all samples were quantified and analyzed for the temperature range of 25 K to 300 K to study the oxygen-induced interface modification in our magnetic stacks. We found the variation in depinning fields and magnetic properties can be attributed to the oxidation of cobalt at the Co/AlO_x interface.

2. Experimental Details

The Pt/Co/AlO_x (t nm) trilayers were deposited on a thermally oxidized silicon substrate by magnetron sputtering at room temperature with a base pressure of about 4×10^{-5} Pa. The sputtered rates of all the target materials were calibrated by using a Bruker Profilometer and found to be around $0.021 \pm 2.5 \times 10^{-4}$ nm/s. The complete thin film stacks from the substrate side were Ta (10 nm)/Pt (4 nm)/Co (1.1 nm)/AlO_x (t nm)/Pt (4 nm), where, t = 3, 3.6, 4.17, 4.58, 5, 5.4, 5.8, and 6.2. Herein, heavy metals Ta (10 nm)/Pt (4 nm) were sputtered first as a buffer or seed layer to boost the PMA [30]. The top Pt layer acts as a capping layer to protect the film from oxidation. The aluminum metal sandwiched in between Co and Pt was oxidized for 17 s at a pressure of 2.93 Pa by using RF power at 40 watts before the deposition of top platinum. Multiple magnetic samples were grown by varying aluminum thicknesses (t_{AlO_x}) and the films post-annealed at 460 °C for 30 min under ultrahigh vacuum to improve the crystallinity and thus promote PMA.

The magnetic characteristics were studied by hysteresis curves obtained from a vibrating sample magnetometer (VSM) and anomalous Hall effect (AHE) systems at room temperature [31]. The dimensions of the sample pieces used in the measurements ranged from 4×4 mm^2 to 4×6 mm^2. In addition, DW motion was studied by using a polar magneto-optical Kerr effect (P-MOKE) microscopy imaging system. For imaging purposes, samples were diced into small pieces, sized around 5 mm^2, and the symmetric domain wall dynamics were investigated by applying out-of-plane (OOP) magnetic fields up to 40 mT. Next, the low-temperature AHE measurements were performed to study the effect of interfacial oxygen on magnetization. For the measurement, the samples were patterned in the form of Hall bar devices by using photolithography and plasma etch techniques. A Keithley 2450 source meter, monitored by LabView software, was used to supply the small current density in the order of 10^{11} A/m^2 to measure the anomalous Hall resistance. The layered structures of our samples were verified by using transmission electron microscopy (TEM) imaging and a morphological study was carried out with the help of atomic force microscopy (AFM) images.

3. Results

3.1. Magnetic Characterization

To find the PMA of the samples, we first extracted hysteresis curves taken from measuring the Hall resistance, R_{Hall}, and magnetization, M, as a function of the OOP magnetic field, H_z, at the room temperature, as displayed in Figure 1a,b. These data show very good perpendicular magnetic anisotropy PMA in the t_{AlO_x} range of 3 to 5.8 nm. However, the easy axis OOP anisotropy directions change into the easy plane at a thickness of 6.2 nm, as displayed in Figure 1a, observed from the AHE measurement. Figure 1c shows the in-plane magnetoresistive behavior of a Pt (4 nm)/Co (1.1 nm)/AlO_x (4.58 nm) sample and the inset in Figure 1c is the Kerr image of the Hall bar device with the measurement scheme. From the hysteresis of Figure 1c, we can easily recognize that R_{Hall} is maximum at the zero in-plane field, H_x, and it begins to decline slowly on increasing the H_x, indicating the prominent magnetization of our sample along the OOP direction [32]. The coercive field H_c anisotropy field, and saturation magnetization, M_s, were extracted from the hysteresis loops in Figure 1b,c. The detailed method to find the magnetization in Figure 1b can be found in our previous work [31]. Similarly, interfacial PMA is given by the effective anisotropy energy density, K_{eff}, and it is extracted by using the relation $K_{eff} = \frac{1}{2}\mu_o H_{an} M_s$, where H_{an} is the effective anisotropy field and is taken as the field corresponding to 90% of the saturated anomalous Hall resistance value on AHE curves with an in-plane field [10,33]. The AlO_x thickness dependence on H_c, M_s, and K_{eff} can be seen in Figure 1d. From Figure 1d, it can be discerned that H_c rises remarkably from 0.68 mT to 13 mT while increasing t_{AlO_x} up to 5 nm-thick AlO_x; then, it starts decreasing. In the same way, M_s is slightly descended for higher t_{Alo_x} and K_{eff} is tuned lying within the range of 7% of its mean value; these small declinations in M_s values may be due to the weak partial oxidation of cobalt at the interface.

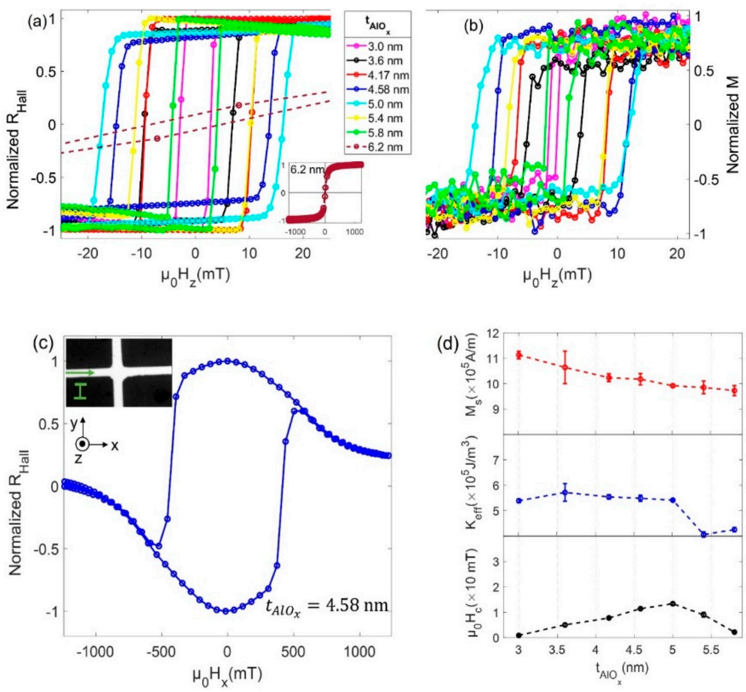

Figure 1. (**a**) Normalized hall resistance, R_{Hall}, as a function of the OOP magnetic field (H_z). The inset on the bottom right is the complete R_{Hall}–H_z loop for the Pt (4 nm)/Co (1.1 nm)/AlO_x (6.2 nm) sample. (**b**) Normalized magnetization (M) against H_z, obtained from the vibration sample magnetometry measurement. (**c**) R_{Hall} as a function of the in-plane field H_x for the Pt (4 nm)/Co (1.1 nm)/AlO_x (4.58 nm) sample. The top left inset is the polar Kerr image of the 27 μm channel width Hall bar device and the green arrow on it gives the direction of the applied current during the measurement. (**d**) Variation in saturation magnetization (red data points), effective anisotropy (blue data points), and coercivity (black data points) with the AlO_x thickness.

3.2. Domain Wall Velocity and Depinning Fields

For the quantification of DW velocity and depinning fields on the magnetic samples, we studied the field-induced symmetric DW motion in the creep regime by using P-MOKE. This method is ideal for understanding the DW dynamics and is convenient without requiring any microfabrication. In our experiment, DW motions were visualized and manipulated by 300 ms to 120 s H_z pulses of discrete amplitudes. The magnetic films were saturated by using a 1-s pulse of amplitude $\pm$ 40 mT H_z and the DWs were nucleated by using opposite fields, which were taken as the reference images, as seen in Figure 2a. For every pulse, the DW displacements were taken as the subtraction of the reference image (Figure 2a) from the DW image after the pulse (Figure 2b). The differential displacement of the magnetic bubble expansion was plotted against the different pulse durations of particular H_z amplitudes. Then, the gradients of the corresponding plots were taken as the DW velocities, which are shown in Figure 2d as a function of t_{AlO_x}. We found that the film containing 5 nm AlO_x has the minimum velocity for all H_z, ranging from −8 mT to +8 mT in 0.2-field point increments. However, the velocity of the 5.8 nm AlO_x sample cannot be recorded in our experiment, as the sample is comprised of weakly pinned magnetic DWs, as shown in Figure 2e.

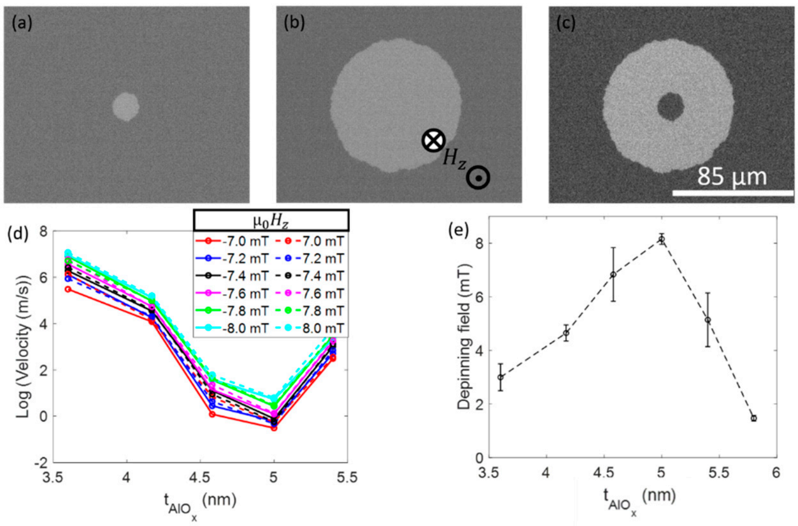

Figure 2. (**a**) Magnetic domain wall (DW) nucleated with a 1-s pulse of the OOP field H_z of −8.5 mT, acting as a reference image. (**b**) DW driven with the 8-s pulse of −7.8 mT H_z. (**c**) Differential image of DW corresponding to (**a**,**b**) of the Pt (4 nm)/Co (1.1 nm)/AlO_x (5.8 nm) sample. (**d**) DW velocity as a function of aluminum oxide thickness, t_{AlO_x}, for the different OOP fields. (**e**) Plot showing dependence of the depinning field on t_{AlO_x}.

By following the same procedure, the depinning fields were evaluated in our system, which is defined as the minimum applied fields at which the DWs start to expand [8], and the accuracy of our measurement system is on the order of 0.6 μm/s. This depinning field dependence on t_{AlO_x} is shown in Figure 2e, and an extremely small depinning field for the 3 nm sample could not be noted because of having extremely small coercivity at room temperature. It was found that the strongest depinning field is for the 5 nm t_{AlO_x} sample and on increasing thickness it starts decreasing following the fashion of coercivity change in Figure 1d. Although this method of finding the depinning field is not very precise, as the DW motion in the creep regime is also thermal energy dependent [34–36], it offers a very good approximation of its alteration trend [8].

3.3. Material and Morphological Characterization

To observe the oxidation content at the interface, low-temperature magneto-transport measurements were carried out in our PMA samples. The magnetoresistive curves (Figure 3a) as a function of H_z show the hysteretic behavior at a low temperature of 35 K. We measured the coercivities for temperatures ranging from 25 K to 300 K for all the OOP anisotropic samples in Figure 3b. In our low-temperature transport measurement system, the switching behavior of the hysteresis loops could also be affected by the Joules heating effect due to the applied current. To minimize such an effect, we applied the smallest possible current and the coercivities were taken as the average of the switching fields for both up–down and down–up DWs.

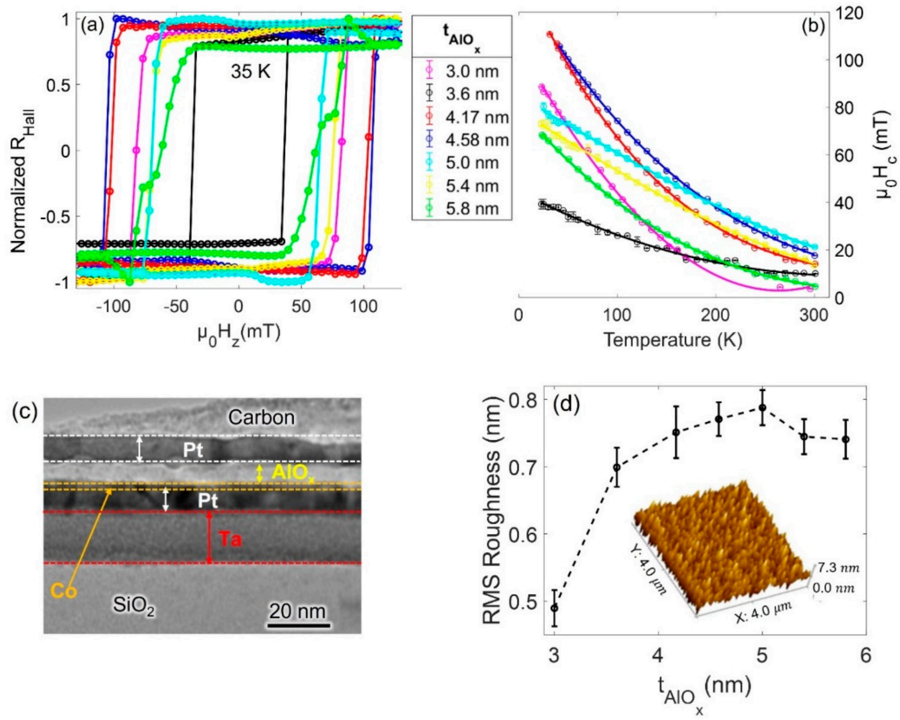

Figure 3. (**a**) Normalized anomalous Hall resistances versus the OOP field H_z for different t_{AlO_x} measured at 35 K temperature. (**b**) Temperature dependence of the coercive fields for the sample of varying aluminum oxide thicknesses. (**c**) Transmission electron microscopy image displaying the layered structure of the Pt (4 nm)/Co (1.1 nm)/AlO_x (4.8 nm) sample. (**d**) Plot showing the roughness of all PMA samples as a function of aluminum oxide thickness. The inset in (**d**) represents the 4×4 μm^2 atomic force microscopy image of Pt (4 nm)/Co (1.1 nm)/AlO_x (4.8 nm).

At the lowest possible temperature in our system, we found that H_c increased with a larger t_{AlO_x} until it reached 4.58 nm, and then began dropping, as shown in Figure 3b. Refs. [18,37] contend that such a trend of transformation of H_c values is the signature of the formation of an antiferromagnetic CoO_x state at the Co/AlO_x interface due to the migration of oxygen along the grain boundaries. However, our 3.6 nm-thick film behaved anomalously, showing very weak coercivity at a low temperature, which may be due to the diffusion of oxygen away from cobalt.

All the material stacks on our thin films are displayed in the TEM image (Figure 3c) of the Pt (4 nm)/Co (1.1 nm)/AlO_x (4.58 nm) trilayer. In this image, cobalt is barely distinguishable because of its very small thickness compared to other components. The RMS values of the roughness of our heterostructured surfaces were measured to be in the range of 0.5 to 0.85 nm from AFM measurements. The inset of Figure 3d shows a 4×4 μm^2 AFM image of the heterostructure with t_{AlO_x} = 4.58 nm, and its roughness was found to be 0.77 ± 0.05 nm. The roughness values of all the PMA samples are displayed in Figure 3d. Although the roughness values of all the measured films are very close, their values slightly declined for films comprising of a higher and lower than 5 nm AlO_x thickness, backing up the variation propensities of coercivity (Figure 1d) and the depinning field (Figure 2e).

The lowest and highest roughness were recorded to be 0.49 ± 0.03 nm and 0.79 ± 0.03 for t_{AlO_x} = 3 nm and 5 nm samples, respectively.

4. Discussion

By using the methods discussed above, we measured the magnetic properties and depinning fields at room temperature and coercivities at the low-temperature range for various t_{AlO_x} of asymmetric Pt/Co/AlO_x trilayer systems; the respective results are provided in Figures 1d, 2e, and 3b. The reason for the difference in the magnetic parameters and non-monotonic behavior of the depinning fields in this result can be twofold: interfacial effects and the surface roughness of the thin films. Regarding interfacial impact, this variation may be attributed to both top Co/AlO_x and bottom Pt/Co interfaces, as claimed by [22]. At a high annealing temperature of 460 °C, the formation of intermetallic CoPt alloy at the bottom interface reduces the pure metallic cobalt, which might affect the magnetization values of the samples [38]. However, our result (Figure 3b) supports that these properties are predominantly determined by the modification of diffusion-caused oxygen content in the top Co/AlO_x interface, where the H_c values of all the samples are increasing on lowering the temperature, which arises due to the exchange coupling between the ferromagnetic Co and antiferromagnetic CoO_x [18].

First, when the aluminum is oxidized after the Co deposition, some of the cobalt can be changed into cobalt oxide thinning of the metallic cobalt, which is responsible for the alteration of both the MOKE and magnetic properties [39]. In addition to that, the enhancement of these quantities by increasing the t_{AlO_x} from 3.6 nm to 5.0 nm may be due to the protection of cobalt from overdegradation by the thicker aluminum, as the magnetic properties are determined by cobalt thickness [40]. On following this trend, abrupt reduction of the depinning field as well as the slight declination of other magnetic properties beyond the critical t_{AlO_x} = 5 nm might be due to the reduction of degree of oxidation at the interface [18]. Such adaptation in oxygen content at the interface is bolstered by low-temperature coercive field measurement results (Figure 3d). On the other hand, the magnetic properties, including the magnetization switching field and DW motion, are highly dependent on the surface roughness of the ultrathin films [41–44]. This fact is bolstered by the aluminum oxide thickness-dependent RMS roughness of the AFM measurements (Figure 3d), which is consistent with the coercivity (Figure 1d) and depinning field (Figure 2e) curves. On further increasing the thickness to 6.2 nm, the easy plane anisotropy direction is switched from perpendicular to in-plane (Figure 3a). This phenomenon occurred because the relatively thicker alumina does not allow enough oxygen to diffuse into the cobalt layer, preventing the Co layer from being thin enough to easily magnetize it along the OOP direction, as PMA is highly sensitive to ferromagnetic film thickness [45].

5. Conclusions

To summarize, we investigated AlO_x thickness dependence on the saturation magnetization, effective anisotropy, and coercivity of the Pt/Co/AlO_x heterostructure by using vibration sample magnetometry and anomalous Hall effect measurement techniques. Although the change in saturation magnetization and anisotropy is very small, a strong dependence of coercivity on AlO_x thickness was observed, recording the maximum at 13 mT for a 5 nm AlO_x. The domain wall depinning fields were quantified by studying the field-driven DW dynamics, using polar MOKE. When the AlO_x thickness is 5 nm, the depinning field is at its maximum, at around 8 mT, and the DW velocity is at its minimum, at 0.6 µm/s. This alteration is attributed to the transformation of the Co/AlO_x interface and the degree of roughness of the films, as supported by the results from the low-temperature (25 K–300 K) magnetoresistance and atomic force microscopy measurement techniques, respectively. These results show the importance of FM layer oxidation to the depinning of chiral DWs in future spintronics devices.

Author Contributions: Conceptualization, B.R.S. and E.T.; investigation B.R.S.; data curation, B.R.S., U.L. and S.M.; writing—original draft, B.R.S.; review and editing, E.T., D.M., R.S. and B.R.S.; supervision, E.T. and D.M.; funding acquisition, E.T. All authors have read and agreed to the published version of the manuscript.

Funding: This work was supported by National Science Foundation (NSF) OIA-1929086.

Institutional Review Board Statement: Not applicable.

Informed Consent Statement: Not applicable.

Data Availability Statement: The data presented in this study are available on request from the corresponding author.

Conflicts of Interest: The authors declare no conflict of interest.

References

1. Tudu, B.; Tiwari, A. Recent developments in perpendicular magnetic anisotropy thin films for data storage applications. *Vacuum* **2017**, *146*, 329–341. [CrossRef]
2. Speetzen, N.; Stadler, B.J.H.; Yuan, E.; Victora, R.H.; Qi, X.; Judy, J.H.; Supper, N.; Pohkil, T. Co/Pd multilayers for perpendicular magnetic recording media. *J. Magn. Magn. Mater.* **2005**, *287*, 181–187. [CrossRef]
3. Honda, N.; Ariake, J.; Ouchi, K.; Iwasaki, S.I. Low noise Co-Cr-Nb perpendicular recording media with high squareness. *IEEE Trans. Magn.* **1998**, *34*, 1651–1653. [CrossRef]
4. Iwasaki, S.I. Perpendicular magnetic recording—Its development and realization. *Proc. Jpn. Acad. Ser. B Phys. Biol. Sci.* **2009**, *85*, 37–54. [CrossRef] [PubMed]
5. Parkin, S.S.P.; Hayashi, M.; Thomas, L. Magnetic domain-wall racetrack memory. *Science* **2008**, *320*, 190–194. [CrossRef]
6. Yu, G.; Upadhyaya, P.; Shao, Q.; Wu, H.; Yin, G.; Li, X.; He, C.; Jiang, W.; Han, X.; Amiri, P.K.; et al. Room-temperature skyrmion shift device for memory application. *Nano Lett.* **2017**, *17*, 261–268. [CrossRef]
7. Thomas, L.; Yang, S.H.; Ryu, K.S.; Hughes, B.; Rettner, C.; Wang, D.S.; Tsai, C.H.; Shen, K.H.; Parkin, S.S.P. Racetrack memory: A high-performance, low-cost, non-volatile memory based on magnetic domain walls. In Proceedings of the 2011 International Electron Devices Meeting, Washington, DC, USA, 5–7 December 2011; pp. 535–538. [CrossRef]
8. Huang, Y.; Li, X.; Wang, L.; Yu, G.; Wang, K.L.; Zhao, W. Interface control of domain wall depinning field. *AIP Adv.* **2018**, *8*, 056314. [CrossRef]
9. Peng, S.; Wang, M.; Yang, H.; Zeng, L.; Nan, J.; Zhou, J.; Zhang, Y.; Hallal, A.; Chshiev, M.; Wang, K.L.; et al. Origin of interfacial perpendicular magnetic anisotropy in MgO/CoFe/Metallic capping layer structures. *Sci. Rep.* **2015**, *5*, 18173. [CrossRef]
10. Johnson, M.T.; Bloemen, P.J.H.; Den Broeder, F.J.A.; De Vries, J.J. Magnetic anisotropy in metallic multilayers. *Rep. Prog. Phys.* **1996**, *59*, 1409–1458. [CrossRef]
11. Belmeguenai, M.; Adam, J.P.; Roussigné, Y.; Eimer, S.; Devolder, T.; Kim, J.V.; Cherif, S.M.; Stashkevich, A.; Thiaville, A. Interfacial Dzyaloshinskii-Moriya interaction in perpendicularly magnetized Pt/Co/AlOx ultrathin films measured by brillouin light spectroscopy. *Phys. Rev. B—Condens. Matter Mater. Phys.* **2015**, *91*, 180405. [CrossRef]
12. Ma, X.; Yu, G.; Razavi, S.A.; Sasaki, S.S.; Li, X.; Hao, K.; Tolbert, S.H.; Wang, K.L.; Li, X. Dzyaloshinskii-Moriya interaction across an antiferromagnet-ferromagnet interface. *Phys. Rev. Lett.* **2017**, *119*, 027202. [CrossRef]
13. Lu, H.M.; Zheng, W.T.; Jiang, Q. Saturation magnetization of ferromagnetic and ferrimagnetic nanocrystals at room temperature. *J. Phys. D: Appl. Phys.* **2007**, *40*, 320–325. [CrossRef]
14. Dimitrov, D.; Zhang, S. Effect of exchange interactions at antiferromagnetic/ferromagnetic interfaces on exchange bias and coercivity. *Phys. Rev. B—Condens. Matter Mater. Phys.* **1998**, *58*, 12090–12094. [CrossRef]
15. Sabet, S.; Moradabadi, A.; Gorji, S.; Fawey, M.H.; Hildebrandt, E.; Radulov, I.; Wang, D.; Zhang, H.; Kübel, C.; Alff, L. Correlation of interface structure with magnetic exchange in a hard/soft magnetic model nanostructure. *Phys. Rev. Appl.* **2019**, *11*, 054078. [CrossRef]
16. Wang, K.; Wu, M.C.; Lepadatu, S.; Claydon, J.S.; Marrows, C.H.; Bending, S.J. Optimization of Co/Pt multilayers for applications of current-driven domain wall propagation. *J. Appl. Phys.* **2011**, *110*, 083913. [CrossRef]
17. Rodmacq, B.; Manchon, A.; Ducruet, C.; Auffret, S.; Dieny, B. Influence of thermal annealing on the perpendicular magnetic anisotropy of Pt/Co/AlOx trilayers. *Phys. Rev. B—Condens. Matter Mater. Phys.* **2009**, *79*, 024423. [CrossRef]
18. Garad, H.; Fettar, F.; Gay, F.; Joly, Y.; Auffret, S.; Rodmacq, B.; Dieny, B.; Ortega, L. Temperature variation of magnetic anisotropy in Pt/Co/AlOx trilayers. *Phys. Rev. Appl.* **2017**, *7*, 034023. [CrossRef]
19. Moore, T.A.; Miron, I.M.; Gaudin, G.; Serret, G.; Auffret, S.; Rodmacq, B.; Schuhl, A.; Pizzini, S.; Vogel, J.; Bonfim, M. High domain wall velocities induced by current in ultrathin Pt/Co/AlOx wires with perpendicular magnetic anisotropy. *Appl. Phys. Lett.* **2008**, *93*, 262504. [CrossRef]
20. Jué, E.; Thiaville, A.; Pizzini, S.; Miltat, J.; Sampaio, J.; Buda-Prejbeanu, L.D.; Rohart, S.; Vogel, J.; Bonfim, M.; Boulle, O.; et al. Domain wall dynamics in ultrathin Pt/Co/AlOx microstrips under large combined magnetic fields. *Phys. Rev. B* **2016**, *93*, 014403. [CrossRef]

21. Ha Pham, T.; Vogel, J.; Sampaio, J.; Vaňatka, M.; Rojas-Sánchez, J.C.; Bonfim, M.; Chaves, D.S.; Choueikani, F.; Ohresser, P.; Otero, E.; et al. Very large domain wall velocities in Pt/Co/GdOx and Pt/Co/Gd trilayers with Dzyaloshinskii-Moriya interaction. *EPL* **2016**, *113*, 67001. [CrossRef]
22. Kim, N.H.; Cho, J.; Jung, J.; Han, D.S.; Yin, Y.; Kim, J.S.; Swagten, H.J.M.; Lee, K.; Jung, M.H.; You, C.Y. Role of top and bottom interfaces of a Pt/Co/AlOx system in Dzyaloshinskii-Moriya interaction, interface perpendicular magnetic anisotropy, and magneto-optical Kerr effect. *AIP Adv.* **2017**, *7*, 035213. [CrossRef]
23. Li, D.; Ma, R.; Cui, B.; Yun, J.; Quan, Z.; Zuo, Y.; Xi, L.; Xu, X. Effect of the oxide layer on the interfacial Dyzaloshinskii-Moriya interaction in perpendicularly magnetized Pt/Co/SmOx and Pt/Co/AlOx heterostructures. *Appl. Surf. Sci.* **2020**, *513*, 145768. [CrossRef]
24. Sankhi, B.R.; Echeverria, E.; Nembach, H.T.; Shaw, J.M.; Mandal, S.; Annaorazov, M.; Sachan, R.; Mcllroy, D.N.; Meyers, D.; Turgut, E. Engineering of heterostructure Pt/Co/AlOx for the enhancement of Dyzaloshinskii-Moria interaction. *arXiv* **2022**, arXiv:2205.15940. [CrossRef]
25. Kang, M.G.; Choi, J.G.; Jeong, J.; Park, J.Y.; Park, H.J.; Kim, T.; Lee, T.; Kim, K.J.; Kim, K.W.; Oh, J.H.; et al. Electric-field control of field-free spin-orbit torque switching via laterally modulated Rashba effect in Pt/Co/AlOx structures. *Nat. Commun.* **2021**, *12*, 7111. [CrossRef] [PubMed]
26. Schott, M.; Ranno, L.; Béa, H.; Baraduc, C.; Auffret, S.; Bernand-Mantel, A. Electric field control of interfacial Dzyaloshinskii-Moriya interaction in Pt/Co/AlOx thin films. *J. Magn. Magn. Mater.* **2021**, *520*, 167122. [CrossRef]
27. Yang, M.; Luo, J.; Ji, Y.; Zheng, H.-Z.; Wang, K.; Deng, Y.; Wu, Z.; Cai, K.; Edmonds, K.W.; Li, Y.; et al. Spin logic devices via electric field controlled magnetization reversal by spin-orbit torque. *IEEE Electron Device Lett.* **2019**, *40*, 1554–1557. [CrossRef]
28. Moodera, J.S.; Kinder, L.R.; Wong, T.M.; Meservey, R. Large magnetoresistance at room temperature in ferromagnetic thin film tunnel junctions. *Phys. Rev. Lett.* **1995**, *74*, 3273–3276. [CrossRef]
29. Liu, R.S.; Michalak, L.; Canali, C.M.; Samuelson, L.; Pettersson, H. Tunneling anisotropic magnetoresistance in Co/AlOx/Au tunnel junctions. *Nano Lett.* **2008**, *8*, 848–852. [CrossRef]
30. Sun, Y.; Ba, Y.; Chen, A.; He, W.; Wang, W.; Zheng, X.; Zou, L.; Zhang, Y.; Yang, Q.; Yan, L.; et al. Electric-field modulation of interface magnetic anisotropy and spin reorientation transition in (Co/Pt)3/PMN-PT heterostructure. *ACS Appl. Mater. Interfaces* **2017**, *9*, 10855–10864. [CrossRef]
31. Sankhi, B.R.; Turgut, E. A low-cost vibrating sample magnetometry based on audio components. *J. Magn. Magn. Mater.* **2020**, *502*, 166560. [CrossRef]
32. Chen, Y.; Zhang, Q.; Jia, J.; Zheng, Y.; Wang, Y.; Fan, X.; Cao, J. Tuning Slonczewski-like torque and Dzyaloshinskii-Moriya interaction by inserting a Pt spacer layer in Ta/CoFeB/MgO structures. *Appl. Phys. Lett.* **2018**, *112*, 232402. [CrossRef]
33. Cao, A.; Zhang, X.; Koopmans, B.; Peng, S.; Zhang, Y.; Wang, Z.; Yan, S.; Yang, H.; Zhao, W. Tuning the Dzyaloshinskii-Moriya interaction in Pt/Co/MgO heterostructures through the MgO thickness. *Nanoscale* **2018**, *10*, 12062–12067. [CrossRef]
34. Jeudy, V.; Mougin, A.; Bustingorry, S.; Savero Torres, W.; Gorchon, J.; Kolton, A.B.; Lemaître, A.; Jamet, J.P. Universal pinning energy barrier for driven domain walls in thin ferromagnetic films. *Phys. Rev. Lett.* **2016**, *117*, 057201. [CrossRef]
35. Caballero, N.B.; Fernández Aguirre, I.; Albornoz, L.J.; Kolton, A.B.; Rojas-Sánchez, J.C.; Collin, S.; George, J.M.; Diaz Pardo, R.; Jeudy, V.; Bustingorry, S.; et al. Excess velocity of magnetic domain walls close to the depinning field. *Phys. Rev. B* **2017**, *96*, 224422. [CrossRef]
36. Diaz Pardo, R.; Savero Torres, W.; Kolton, A.B.; Bustingorry, S.; Jeudy, V. Universal depinning transition of domain walls in ultrathin ferromagnets. *Phys. Rev. B* **2017**, *95*, 184434. [CrossRef]
37. Garad, H.; Ortega, L.; Ramos, A.Y.; Joly, Y.; Fettar, F.; Auffret, S.; Rodmacq, B.; Diény, B.; Proux, O.; Erko, A.I. Competition between CoOx and CoPt phases in Pt/Co/AlO x semi tunnel junctions. *J. Appl. Phys.* **2013**, *114*, 053508. [CrossRef]
38. Myagkov, V.G.; Bykova, L.E.; Zhigalov, V.S.; Matsynin, A.A.; Velikanov, D.A.; Bondarenko, G.N. Solid-state synthesis, rotatable magnetic anisotropy and characterization of $Co_{1-x}Pt_x$ phases in 50Pt/50fccCo(001) and 32Pt/ 68fccCo(001) thin films. *J. Alloys Compd.* **2021**, *861*, 157938. [CrossRef]
39. Silva, E.F.; Corrêa, M.A.; Della Pace, R.D.; Plá Cid, C.C.; Kern, P.R.; Carara, M.; Chesman, C.; Alves Santos, O.; Rodríguez-Suárez, R.L.; Azevedo, A.; et al. Thickness dependence of the magnetic anisotropy and dynamic magnetic response of ferromagnetic NiFe films. *J. Phys. D. Appl. Phys.* **2017**, *50*, 185001. [CrossRef]
40. Jafri, Y.; Sharma, G.; Gupta, A.; Gupta, M.; Reddy, V.R. Thickness dependent magnetic properties of ferromagnetic films (Fe, Co) interfaced with Ta. *Thin Solid Films* **2021**, *719*, 138490. [CrossRef]
41. Jiang, Q.; Yang, H.N.; Wang, G.C. Effect of interface roughness on hysteresis loops of ultrathin Co films from 2 to 30 ML on Cu(001) surfaces. *Surf. Sci.* **1997**, *373*, 181–194. [CrossRef]
42. Zhao, Y.P.; Gamache, R.M.; Wang, G.C.; Lu, T.M.; Palasantzas, G.; De Hosson, J.T.M. Effect of surface roughness on magnetic domain wall thickness, domain size, and coercivity. *J. Appl. Phys.* **2001**, *89*, 1325–1330. [CrossRef]
43. Martinez, E. The stochastic nature of the domain wall motion along high perpendicular anisotropy strips with surface roughness. *J. Phys. Condens. Matter* **2012**, *24*, 024206. [CrossRef] [PubMed]
44. Shaw, J.M.; Nembach, H.T.; Silva, T.J. Roughness induced magnetic inhomogeneity in Co/Ni multilayers: Ferromagnetic resonance and switching properties in nanostructures. *J. Appl. Phys.* **2010**, *108*, 093922. [CrossRef]
45. Lourembam, J.; Ghosh, A.; Zeng, M.; Wong, S.K.; Yap, Q.J.; Ter Lim, S. Thickness-dependent perpendicular magnetic anisotropy and gilbert damping in Hf/Co20Fe60 B20/Mg O heterostructures. *Phys. Rev. Appl.* **2018**, *10*, 044057. [CrossRef]